Original Article

Golden-angle radial sparse parallel (GRASP) magnetic resonance angiography (MRA) for endoleak evaluation after endovascular repair of the aorta: a prospective comparison to conventional time-resolved MRA

Haidara Almansour[1], Migdat Mustafi[2], Mario Lescan[3], Ulrich Grosse[4], Mateja Andic[5], Jörg Schmehl[1], Christoph Artzner[1,6], Gerd Grözinger[1], Sven S. Walter[1]

[1]Department of Diagnostic and Interventional Radiology, Eberhard Karls University Tuebingen, University Hospital Tuebingen, Tübingen, Germany; [2]Klinik für Thoraxchirurgie-Lungentransplantation und Klinik für Kinderherzchirurgie, Universitätsklinikum des Saarlandes, Homburg, Germany; [3]Department of Cardiovascular Surgery, University Hospital Freiburg, Freiburg, Germany; [4]Department of Radiology, Cantonal Hospital Frauenfeld, Frauenfeld, Switzerland; [5]Department of Thoracic and Cardiovascular Surgery, University Hospital Tübingen, Tübingen, Germany; [6]Diakonie Klinikum Stuttgart, Department of Radiology, Stuttgart, Germany

Contributions: (I) Conception and design: H Almansour, U Grosse, J Schmehl, C Artzner, G Grözinger, SS Walter; (II) Administrative support: All authors; (III) Provision of study materials or patients: All authors; (IV) Collection and assembly of data: H Almansour, M Mustafi, M Lescan, U Grosse, M Andic, C Artzner, G Grözinger, SS Walter; (V) Data analysis and interpretation: H Almansour, J Schmehl, C Artzner, G Grözinger, SS Walter; (VI) Manuscript writing: All authors; (VII) Final approval of manuscript: All authors.

Correspondence to: Sven S. Walter, MD. Department of Diagnostic and Interventional Radiology, Eberhard Karls University Tuebingen, University Hospital Tuebingen, Hoppe-Seyler-Straße 3, 72076 Tübingen, Germany. Email: sven.walter@med.uni-tuebingen.de.

Background: Time-resolved angiography with interleaved stochastic trajectories (TWIST) magnetic resonance angiography (MRA) may obscure smaller vessels and is highly susceptibility to motion artifacts, potentially reducing endoleak detection accuracy after endovascular aortic repair (EVAR). The novel golden-angle radial sparse parallel (GRASP) sequence enhances spatial and temporal resolution with continuous, motion-robust datasets, showing promise for accurate endoleak detection post-EVAR. This study aimed to compare the diagnostic effectiveness of contrast-enhanced compressed-sensing radial GRASP-volume interpolated breath-hold examination (VIBE) sequence with standard contrast-enhanced dynamic TWIST-VIBE sequence in patients with inconclusive computed tomography angiography (CTA) findings regarding endoleak after EVAR.

Methods: This single-center prospective study consecutively enrolled adults with inconclusive findings regarding the presence or type of endoleak in multiphasic CTA following EVAR for abdominal aortic aneurysms. Participants underwent contrast-enhanced MRA, acquiring dynamic TWIST-VIBE and GRASP-VIBE sequences. Two independent radiologists assessed the datasets for image quality, diagnostic confidence, and the presence and type of endoleak. Additionally, quantitative assessments with signal-to-noise ratios (SNR) and contrast-to-noise ratios (CNR) were performed. Statistical analyses included interrater and intermethod agreement, and diagnostic performance testing.

Results: Twenty participants (mean age, 72±9 years; 13 males) were included. GRASP-VIBE demonstrated superior image quality over TWIST-VIBE sequence with predominantly absent motion artifacts and increased diagnostic confidence (all P<0.001). Diagnostic performance significantly improved for detecting type II endoleaks in GRASP-VIBE compared to TWIST-VIBE scans [area under the curve (AUC): 0.96 *vs.* 0.73; P=0.04]. Diagnostic accuracy improved with GRASP-VIBE for overall (AUC: 0.94 *vs.* 0.79) and endoleak type I detection (AUC: 1.0 *vs.* 0.90), however, not significantly (P≥0.05). TWIST-VIBE sequences demonstrated significantly higher SNR for measurements in the clotted aneurysm sac (P=0.01).

No significant differences were observed in CNR for the aorta and any aneurysm sacs across the compared imaging sequences.

Conclusions: Compressed-sensing dynamic GRASP-VIBE sequence, with its superior image quality, diagnostic confidence, and performance, may be preferred over standard TWIST-VIBE sequence in inconclusive endoleak cases.

Keywords: Magnetic resonance angiography (MRA); endovascular aortic repair (EVAR); endoleak; aortic aneurysm

Submitted Jun 06, 2024. Accepted for publication Sep 04, 2024. Published online Sep 26, 2024.
doi: 10.21037/qims-24-1130
View this article at: https://dx.doi.org/10.21037/qims-24-1130

Introduction

Abdominal aortic aneurysms can be managed through minimally invasive endovascular aortic repair (EVAR). This technique involves the deployment of a covered stent-graft to stabilize the aneurysm sac, redirecting blood flow and preventing further expansion (1,2). Although EVAR reduces recovery time and lowers 30-day mortality compared to open surgery, its short-term benefits may be offset by potential long-term complications (3,4). Endoleaks are among the most significant complications, occurring in 20–50% of cases. They are characterized by persistent blood flow into the aneurysm sac outside the stent-graft lumen. Without ongoing lifelong surveillance, there is a risk of progressive expansion of the aneurysm sac, which could potentially lead to aortic rupture (1,3,4). Thus, timely detection and characterization of endoleaks are crucial for guiding clinical management and ensuring patient safety (2,4,5). Identifying the specific type of endoleak is particular important, as each type has different clinical significance and treatment options. Moreover, the endoleak types can affect the short- and long-term outcome of EVAR, making accurate diagnosis essential for optimal patient care (6,7).

For imaging high-flow vessels, time-resolved dynamic magnetic resonance angiography (MRA) is a viable option for post-EVAR surveillance, complementing the established standard of care, triple-phase computed tomography angiography (CTA) (2,3,8). One established MRA technique is the time-resolved angiography with interleaved stochastic trajectories (TWIST). This method employs a view-sharing technique that leverages parallel imaging acceleration and Cartesian k-space trajectories for data undersampling (9,10). Using keyhole imaging the center of the k-space will be imaged more frequently than the peripheral sections resulting in high temporal resolution (11). However, a major disadvantage of the keyhole sampling technique can be the masking of smaller vessels, including their hemodynamics, particularly in the peripheral anatomic regions (11). Further disadvantages of TWIST MRA can be related to image quality with motion artifacts, blurring, and ghosting (11).

The fairly novel dynamic golden-angle radial sparse parallel (GRASP) magnetic resonance imaging (MRI) sequence enables a sparse sampling of the k-space by utilizing a radial acquisition trajectory with a golden-angle increment (9,12-15). The benefit of the golden-angle rotation scheme is the ability to acquire continuous and motion robust MR datasets, allowing for flexibility in data sorting and retrospective temporal resolution adjustment, eliminating the need for the patient's respiratory cooperation (13,15). Additionally, the inherent incoherent undersampling characteristic of radial imaging can be utilized in sparsity-based advanced iterative reconstruction methods, such as compressed sensing, to achieve highly accelerated data acquisitions with enhanced spatial and temporal resolution (9,12-16). These advantages may reveal its potential for accurate and efficient surveillance in detecting endoleaks following EVAR procedures.

The purpose of this study was to compare the diagnostic effectiveness of compressed-sensing radial GRASP sequence with standard dynamic TWIST sequence in patients with inconclusive CTA findings regarding endoleak after EVAR. We represent this article in accordance with the STARD reporting checklist (available at https://qims.amegroups.com/article/view/10.21037/qims-24-1130/rc).

Methods

Study design and study participants

Between April 2018 and October 2023, consecutive

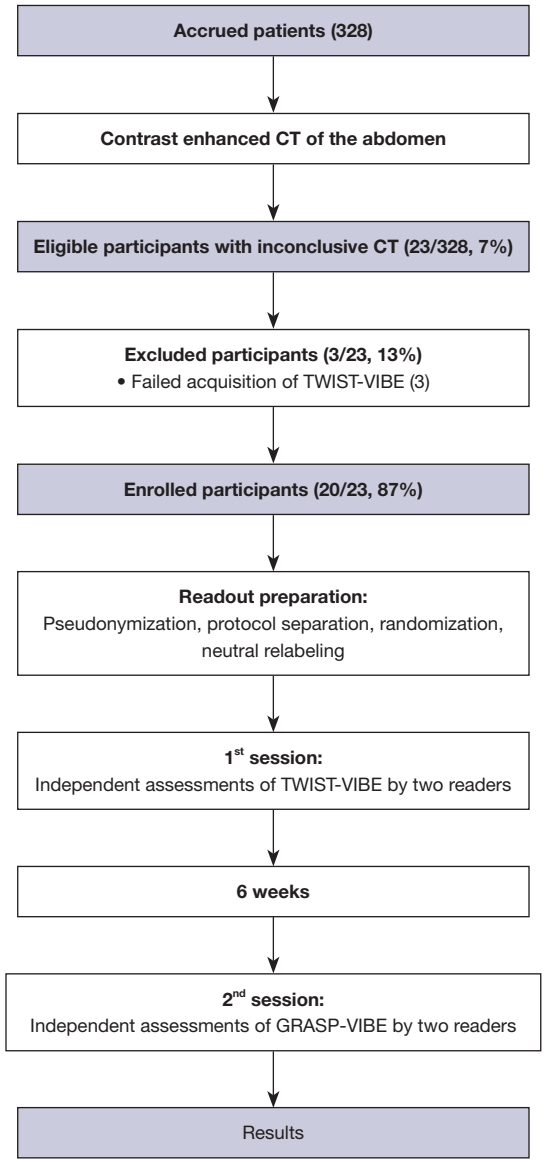

Figure 1 The study's flow chart. CT, computed tomography; TWIST-VIBE, time-resolved angiography with interleaved stochastic trajectories-volume interpolated breath-hold examination; GRASP-VIBE, golden-angle radial sparse parallel-volume interpolated breath-hold examination.

patients referred from the affiliated department of vascular surgery at the University Hospital of Tuebingen who had undergone EVAR were considered for inclusion in this prospective single-center study. The study received approval from the local institutional review board of the University of Tuebingen (No. 166/2018BO2). All participants provided written informed consent prior to their involvement of the study. The study was conducted in accordance with the Declaration of Helsinki (as revised in 2013). Furthermore, we ensured full compliance with the regulations set forth by the Health Insurance Portability and Accountability Act (HIPAA).

Patients with inconclusive radiological findings regarding the diagnosis of an endoleak or regarding the type of endoleak in CTA underwent additional MRI including dynamic sequences. Only patients who were ≥18 years old were included in the study. Patients were excluded if (I) patients refused to participate/undergo MRI, (II) had contraindications for the application of contrast agent, and (III) had contraindications for MRI. *Figure 1* illustrates the inclusion and exclusion process of the study participants.

Some study participants were previously included in an earlier publication (17) that investigated the clinical feasibility of the GRASP-VIBE sequence compared to CTA. In that study, neither the TWIST-VIBE sequence was analyzed nor was a quantitative analysis of the GRASP-VIBE sequence conducted.

MR angiography protocols

In the same session, each participant underwent a contrast enhanced MR angiography acquiring a time-resolved angiography with interleaved stochastic trajectories-volume interpolated breath-hold examination (TWIST-VIBE) and golden-angle radial sparse parallel-volume interpolated breath-hold examination (GRASP-VIBE) sequence on a clinical 3T scanner (Magnetom Vida, Magnetom Vida Fit; all Siemens Healthineers, Forchheim, Germany). The scanners were equipped with a commercially available 18-channel surface body coil with a 72-channel spine coil (Siemens Healthineers, Forchheim, Germany). A body weight adapted bolus of contrast agent (0.1 mL/kg) was administered twice during the MRI protocol, once before the acquisition of TWIST-VIBE and once before the acquisition of GRASP-VIBE (minimum of 8 mL Gadobutrol for both MRA techniques; Gadovist, Bayer Healthcare, Leverkusen, Germany). Each of the two injections were performed using a double syringe power injector with a flow rate of at least 1.5 mL/s followed by a saline flush of 20 mL. The acquisition parameters of the dynamic GRASP-VIBE and TWIST-VIBE sequence are shown in *Table 1*.

Image analysis and readouts

A qualitative and quantitative assessment of pseudo-

Table 1 Acquisition parameters for the dynamic GRASP-VIBE and TWIST-VIBE sequences

Parameter	GRASP-VIBE	TWIST-VIBE
Acquisition time (min:sec)	2:54	2:36
Temporal resolution (sec)	3.1	2.49
Voxel size (mm^3)	0.9×0.9×3.0	0.7×0.7×3.0
Averages	1	1
Slice thickness (mm)	3	3
Number of slices per slab	72	72
Repetition time (ms)	3	3.8
Echo time (ms)	1.57	1.23/2.46
Flip angle (degree)	15	10
Bandwidth (Hz/Px)	980	1,090

GRASP-VIBE, golden-angle radial sparse parallel-volume interpolated breath-hold examination; TWIST-VIBE, time-resolved angiography with interleaved stochastic trajectories-volume interpolated breath-hold examination; Hz, Hertz; Px, pixel.

anonymised MR images was performed independently in a blinded and randomized manner.

The qualitative image analysis was performed by two board-certified radiologists with 5 years (H.A.) and 8 years (S.S.W.) of experience in vascular imaging. The quantitative image analysis was performed by one reader (S.S.W.). The assessment took place in a certified reading room, outfitted with a 32" diagnostic-quality display and a commercially available picture archiving and communication system (Syngo.Via Enterprise Browser Version 2.3.1, Siemens Healthineers, Forchheim, Germany). Each reader utilized their personalized reading preferences, which included customized window and level settings, as well as magnification options.

Qualitative image analysis

The outcome parameters of the qualitative image analysis were motion, artifacts, image noise, edge sharpness, contrast resolution, fat suppression, partial volume effect and overall image quality for TWIST-VIBE and GRASP-VIBE, respectively. Each outcome variable was graded using a visual 5-point Likert score (1= very bad; 2= bad/severe; 3= adequate; 4= good/mild; 5= very good/none). Finally, the diagnostic confidence regarding whether an endoleak was present or absent was evaluated in a similar manner using a 5-point Likert score (1= not confident; 2= low confidence; 3= moderately confident; 4= confident; 5= highly confident).

Detection and classification of endoleaks

Both readers, who conducted the qualitative analysis evaluated all MR examinations independently regarding the presence or absence of endoleaks. If an endoleak was detected, the observer had classify it based on the Cardiovascular and Interventional Radiological Society of Europe (CIRSE) guidelines into five types: (I) endoleak occurring at the attachment points of the endovascular prosthesis (Ia: proximal end; Ib: distal end), (II) backward flow through smaller branch vessels, (III) malfunction of the implanted graft , (IV) porosity of the graft material, and (V) expansion of the aneurysm sack with no visible endoleak (18).

The reference standard for the diagnosis and classification of endoleaks was an experienced interventional radiologist (G.G.), with 13 years of expertise in vascular imaging and treatment, who was not involved in the initial assessments, and had unrestricted access to the entire patient information. The information included clinical information, radiology reports, imaging data, and related treatments from the initial EVAR implantation to the latest follow-up (February 2024) (17). After meticulously reviewing these elements, a conclusion regarding the existence and classification of endoleaks was made.

Quantitative image analysis

The quantitative outcome measures included signal-to-noise (SNR) and contrast-to-noise (CNR) ratios on contrast-enhanced morphologic TWIST-VIBE and GRASP-VIBE sequences. Measurements consisted of the aorta (at the level of the endovascular stent in the repaired aneurysm), clotted part of the aneurysm sac, subcutaneous fat (lower right back at the level of L3), muscle (right psoas muscle), and bone (3rd lumbar vertebra). If an endoleak was present measurements also included the perfused part of the aneurysm sac. Circular regions of interest (ROIs) of 0.25 cm^2 were drawn and copied at identical corresponding locations on both TWIST-VIBE and GRASP-VIBE sequences, utilizing the average pixel value to represent signal intensity. The respective background noise was determined by placing a ROI anterior of the skin surface of the abdomen without influence of artifacts. SNR was calculated as signal intensity of tissue divided by the standard deviation (SD) of the background noise. CNR was determined as [SNR (tissue 1) – SNR (tissue 2)]/SD noise.

Table 2 Demographic characteristics of the cohort

Characteristics	Value (n=20)
Age (y)	72±9
Sex	
Female	4 [20]
Male	16 [80]
BMI (kg/m^2)	26±3
GFR (mL/min/1.73 m^2)	70±21
Postoperative EVAR-related symptoms	
Yes	2 [10]
No	18 [90]
Nitinol-based stent graft	20 [100]
Time interval EVAR-MRI (m)	33±42
Patients undergoing angiography	8 [40]
Time interval MRI-last follow-up (m)	30±25

Data are presented as mean ± standard deviation or number [%]. y, years; BMI, body mass index; GFR, glomerular filtration rate; EVAR, endovascular aortic repair; m, months; MRI, magnetic resonance imaging.

Statistical analysis

Continuous variables are reported as mean ± SD or in number of participants with percentage. The visual Likert-scale assessment of image quality parameters was reported as median, minimum, first to third quartiles (interquartile range, IQR), and maximum values. The paired Wilcoxon signed-rank test was used to compute differences between the two raters or the evaluated MRI sequences. Furthermore, Kendall's Tau (image quality) and Cohen's kappa were used to assess interrater and intermethod agreements. To evaluate diagnostic performance, sensitivity, specificity, and area under the curves (AUCs) were calculated based on reference standard mentioned above. Statistical significance was defined as $P<0.05$ using two-tailed testing.

Statistical analysis was performed using commercially available software (SPSS, IBM Statistics Version 29, Armonk, New York, USA).

Results

Participant characteristics

A total of 328 patients underwent CTA to follow up EVAR of an abdominal aortic aneurysm. Of those, 23 participants demonstrated inconclusive findings for the presence or type of endoleak and underwent additional dynamic MRA (*Figure 1*). After the exclusion of 3 participants due to failed acquisition of the TWIST-VIBE sequence, the final cohort comprised 20 participants (mean age ± SD: 72±9 years). Further details about participant characteristics are shown in *Table 2*.

Image quality

The results of the image quality analysis are provided in *Table 3*. The overall image quality of the GRASP-VIBE sequences was rated significantly better than the TWIST-VIBE sequences [median: 5 (IQR: 4, 4) *vs.* 3 (IQR: 3, 4); $P<0.004$]. There was a significant reduction in motion artifacts for GRASP-VIBE sequences compared to TWIST-VIBE sequences [median: 5 (IQR: 4, 5) *vs.* 3 (IQR: 2, 3); $P<0.001$]. Furthermore, the GRASP-VIBE scans demonstrated significantly less artifacts [median: 4 (IQR: 3, 4) *vs.* 3 (IQR: 2, 4); $P=0.01$] and partial volume effect [median: 4 (IQR: 4, 4) *vs.* 4 (IQR: 3, 4); $P=0.02$], as well as significantly better edge sharpness [median: 4 (IQR: 4, 4) *vs.* 3 (IQR: 3, 4); $P=0.02$], and diagnostic confidence [median: 5 (IQR: 4, 5) *vs.* 4 (IQR: 3, 4); $P<0.001$].

The agreements of the image quality analysis between the raters were at least good for TWIST-VIBE scans [$k\geq0.67$; 95% confidence interval (CI): 0.40–0.94] and very good for the GRASP-VIBE scans ($k\geq0.80$; 95% CI: 0.56–1.0).

Frequencies of endoleaks

The detection frequency and type of endoleak along with the intermethod agreements are provided in *Table 4*. Apart from a moderate agreement in type II endoleaks ($k=0.56$; 95% CI: 0.12–0.89), the intermethod agreement demonstrated good to very good agreements (≥0.62; 95% CI: 0.0–1.0) between the respective sequences.

Diagnostic performance

The numerical results of the diagnostic performance analysis are provided in *Table 5*.

The diagnostic accuracy for overall endoleak detection (AUC: 0.94 *vs.* 0.79) and endoleak type I detection (AUC: 1.0 *vs.* 0.90) had improved with dynamic GRASP-VIBE sequences compared to TWIST-VIBE sequences. Yet, the results were not significant ($P\geq0.08$). Analyzing type I endoleaks in their subclassification showed comparable

Table 3 Comparison of the Likert-scores for TWIST-VIBE and GRASP-VIBE sequences for both readers

Parameters	Rater 1*			Rater 2*			Interrater agreement†	
	TWIST	GRASP	P	TWIST	GRASP	P	TWIST	GRASP
Motion	3 [2, 2–3, 5]	5 [4, 4–5, 5]	<0.001‡	3 [2, 2–3, 5]	5 [4, 5–5, 5]	<0.001‡	0.84 (0.66–1.0)	0.87 (0.63–1.0)
Artifacts	3 [2, 2–4, 4]	4 [2, 3–4, 5]	0.01‡	3 [1, 2–4, 5]	4 [2, 3–5, 5]	0.008‡	0.80 (0.55–1.0)	0.86 (0.68–1.0)
Image noise	4 [3, 4–4, 5]	4 [3, 4–4, 5]	0.75	4 [2, 3–4, 5]	4 [3, 4–5, 5]	0.12	0.67 (0.45–0.88)	0.88 (0.72–1.0)
Edge sharpness	3 [3, 3–4, 5]	4 [3, 4–4, 5]	0.02‡	3 [2, 3–4, 5]	4 [3, 4–4, 5]	<0.001‡	0.72 (0.49–0.94)	0.83 (0.62–1.0)
Contrast resolution	4 [3, 3–4, 5]	4 [3, 3–4, 5]	0.78	4 [3, 3–4, 4]	4 [3, 3–5, 5]	0.76	0.69 (0.45–0.93)	0.86 (0.68–1.0)
Fat suppression	5 [5, 5–5, 5]	5 [5, 5–5, 5]	>0.99	5 [5, 5–5, 5]	5 [5, 5–5, 5]	>0.99	1.0 (1.0–1.0)	1.0 (1.0–1.0)
Partial volume effect	4 [2, 3–4, 4]	4 [3, 4–4, 5]	0.02‡	4 [3, 4–4, 4]	4 [4, 4–5, 5]	0.008‡	0.67 (0.40–0.94)	0.83 (0.64–1.0)
Overall image quality	3 [2, 3–4, 5]	5 [3, 4–4, 5]	0.004‡	3 [1, 3–4, 5]	4 [3, 4–4, 5]	0.002‡	0.80 (0.64–0.95)	0.80 (0.56–1.0)
Diagnostic confidence	4 [2, 3–4, 5]	5 [3, 4–5, 5]	<0.001‡	4 [2, 3–4, 5]	5 [3, 4–5, 5]	<0.001‡	0.88 (0.80–0.96)	0.82 (0.57–1.0)

*, based on a 5-point Likert scale (1= very bad; 5= very good). Values are given as median value with the minimum, first to third quartiles, and maximum; †, data are k values with 95% confidence interval in square bracket; ‡, significant P values. TWIST-VIBE, time-resolved angiography with interleaved stochastic trajectories-volume interpolated breath-hold examination; GRASP-VIBE, golden-angle radial sparse parallel-volume interpolated breath-hold examination; TWIST, time-resolved angiography with interleaved stochastic trajectories; GRASP, golden-angle radial sparse parallel.

Table 4 Rater assessment for the presence and type of endoleak with TWIST-VIBE and GRASP-VIBE

Abnormality*	Reference standard†	Rater 1			Rater 2		
		Frequency (n=20)†		Intermethod agreement‡	Frequency (n=20)†		Intermethod agreement‡
		TWIST	GRASP		TWIST	GRASP	
Endoleak	12 [60]	12 [60]	13 [65]	0.68 (0.30–1.0)	11 [55]	12 [60]	0.69 (0.34–1.0)
Type I	5 [42]	4 [33]	5 [39]	0.86 (0.46–1.0)	6 [46]	5 [42]	0.88 (0.52–1.0)
Ia	1 [20]	2 [50]	1 [20]	0.64 (0.0–1.0)	2 [33]	1 [20]	0.64 (0.0–1.0)
Ib	4 [80]	2 [50]	4 [80]	0.62 (0.0–1.0)	4 [67]	4 [80]	0.69 (0.34–1.0)
Type II	6 [50]	7 [59]	7 [54]	0.56 (0.12–0.89)	4 [36]	6 [50]	0.47 (0.00–0.88)
Type III	1 [8]	1 [8]	1 [7]	1.0 (1.0–1.0)	1 [18]	1 [8]	1.0 (1.0–1.0)

*, no type IV or V endoleaks were seen; †, data in square bracket are percentage; ‡, data are k values with 95% confidence interval in parenthesis. TWIST-VIBE, time-resolved angiography with interleaved stochastic trajectories-volume interpolated breath-hold examination; GRASP-VIBE, golden-angle radial sparse parallel-volume interpolated breath-hold examination; TWIST, time-resolved angiography with interleaved stochastic trajectories; GRASP, golden-angle radial sparse parallel.

diagnostic performance between TWIST-VIBE and GRASP-VIBE scans for type Ia endoleaks with AUC 0.97 and AUC 1.0, respectively (P≥0.99) (*Figure 2*). Diagnostic accuracy for type Ib endoleaks was lower for TWIST-VIBE sequences (AUC: 0.75) compared to GRASP-VIBE (AUC: 1.0), however, not significantly (P=0.08). The detection of type II endoleaks was significantly more accurate with dynamic GRASP-VIBE sequences than with dynamic TWIST-VIBE sequences (AUC: 0.96 *vs.* 0.73; P=0.04) (*Figure 3*). Dynamic TWIST-VIBE and GRASP-VIBE performed the same for diagnosing type III endoleaks (AUC: 1.0 *vs.* 1.0; P>0.99).

Except for type III endoleaks the interrater agreements for endoleaks in general, type I and type II endoleaks demonstrated higher agreements for dynamic GRASP-VIBE scans (k≥0.89) than TWIST-VIBE scans (k≥0.63).

Table 5 Diagnostic performance

Abnormality** and sequence	Interrater agreement‡	No. of findings*				Sensitivity (%)	Specificity (%)	AUC	P
		TP	FP	TN	FN				
Endoleak									0.08
TWIST	0.80 [0.50–1.0]	10	2	6	2	83 [52–98]	75 [35–97]	0.79 [0.60–0.99]	
GRASP	0.89 [0.63–1.0]	12	1	7	0	100 [74–100]	88 [47–100]	0.94 [0.82–0.100]	
EL type I									0.32
TWIST	0.74 [0.34–1.0]	4	0	15	1	80 [28–99]	100 [78–100]	0.90 [0.70–1.0]	
GRASP	1.0 [1.0–1.0]	5	0	15	0	100 [48–100]	100 [78–100]	1.0 [1.0–1.0]	
Type Ia									>0.99
TWIST	0.44 [0.0–1.0]	1	1	18	0	100 [3–100]	95 [74–100]	0.97 [0.73–1.0]	
GRASP	1.0 [1.0–1.0]	1	0	19	0	100 [3–100]	100 [82–100]	1.0 [1.0–1.0]	
Type Ib									0.08
TWIST	0.23 [0.0–0.77]	2	0	16	2	50 [7–93]	100 [79–100]	0.75 [0.47–1.0]	
GRASP	1.0 [1.0–1.0]	4	0	16	0	100 [40–100]	100 [79–100]	1.0 [1.0–1.0]	
EL type II									0.04§
TWIST	0.63 [0.22–1.0]	4	3	11	2	67 [22–96]	78 [49–95]	0.73 [0.49–0.96]	
GRASP	0.89 [0.60–1.0]	6	1	13	0	100 [54–100]	93 [66–100]	0.96 [0.89–1.0]	
EL type III									>0.99
TWIST	1.0 [1.0–1.0]	1	0	19	0	100 [3–100]	100 [82–100]	1.0 [1.0–1.0]	
GRASP	1.0 [1.0–1.0]	1	0	19	0	100 [3–100]	100 [82–100]	1.0 [1.0–1.0]	

Data in parenthesis are 95% confidence intervals. *, data are given in number of patients (n=20); **, no type IV or V endoleaks were seen; ‡, data are k values; §, significant P values. TP, true-positive; FP, false-positive; TN, true-negative; FN, false-negative; AUC, area under the curve; TWIST, time-resolved angiography with interleaved stochastic trajectories; GRASP, golden-angle radial sparse parallel; EL, endoleak.

Type III endoleaks had comparable interrater agreements with k=1.0 for both sequences. Examining type I endoleaks demonstrated good (k=0.74) and perfect agreement (k=1.0) for TWIST-VIBE and GRASP-VIBE sequences, respectively. Subclassified the agreements were fair (k=0.23) for type Ib endoleaks and moderate (k=0.44) for type Ia endoleaks with TWIST-VIBE sequences, while perfect agreement was observed for GRASP-VIBE (k=1.0).

Quantitative analysis

SNR and CNR of different tissues of TWIST- and GRASP-VIBE sequences, and their comparison are shown in *Figure 4*. TWIST-VIBE sequences demonstrated significantly higher SNR for measurements in the clotted aneurysm sac (P=0.01), muscle (P=0.006), and bone (P=0.04). The measurements in the aorta, fat, and if present in the perfused part of the aneurysm sac did not show significantly different values between the compared sequences.

On TWIST-VIBE images the muscle-to-bone CNR (P<0.001) and muscle-to-fat CNR (P=0.003) were significantly higher than in GRASP-VIBE. However, there was no significant difference in CNR regarding measurements of the aortic vessel and the perfused or clotted aneurysm sac.

Discussion

This study aimed to compare the effectiveness of two dynamic contrast-enhanced MRA sequences in the detection and classification of equivocal endoleaks, as identified on CTA scans of patients with abdominal aortic

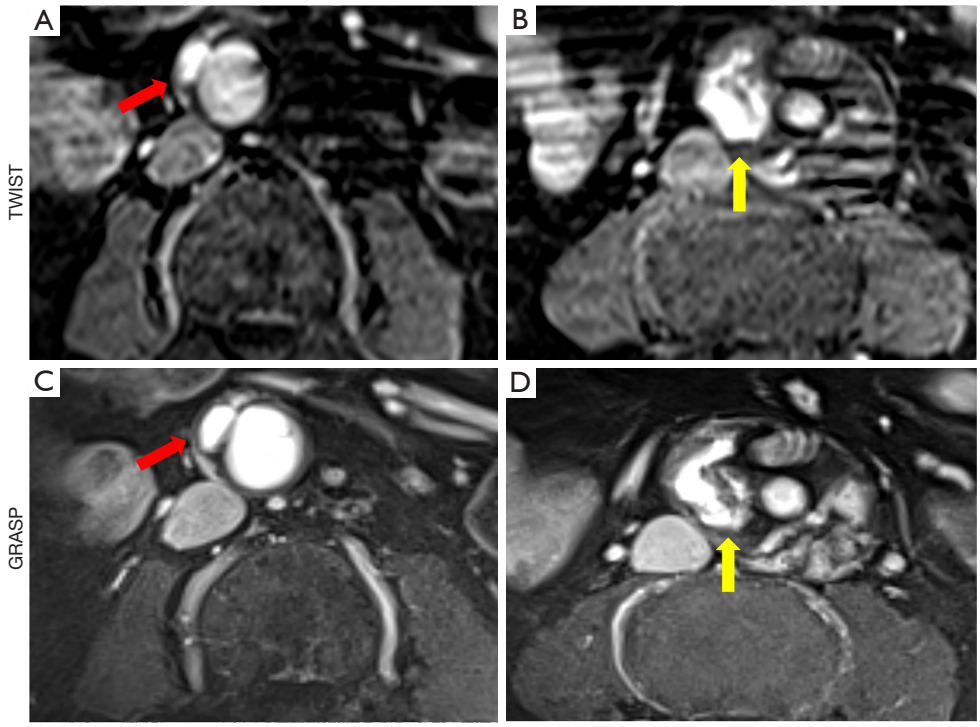

Figure 2 Follow-up imaging after EVAR with Y-Prosthesis in an infrarenal abdominal aortic aneurysm in an 80-year-old man. Both sequences led to the same diagnosis (type Ia endoleak). However, the images acquired by the GRASP sequence show significantly less motion artifacts, higher edge sharpness and a higher overall image quality. (A,B) Axial images acquired by the TWIST sequence showing contrast medium enhancement of the thrombosed aneurysm sac starting at the cranial end of the EVAR stent (red arrow). (B) Increasing contrast medium accumulation with further spread in the aneurysm sac caudally (yellow arrow), which led to the diagnosis of a type Ia endoleak. (C,D) Axial images acquired by the GRASP sequence showing the same findings [red arrow in (C) showing contrast enhancement of the thrombosed sac cranially and yellow arrow in (D) showing increasing contrast medium accumulation caudally], which also led to the diagnosis of a type Ia endoleak. TWIST, time-resolved angiography with interleaved stochastic trajectories; GRASP, golden-angle radial sparse parallel; EVAR, endovascular aortic aneurysm repair.

aneurysms treated with EVAR. Our findings show that the overall image quality of the GRASP-VIBE sequences was significantly better than the TWIST-VIBE sequences with significantly reduced motion artifacts. Furthermore, the diagnostic confidence was higher for GRASP-VIBE than TWIST-GRASP. The diagnostic performance significantly improved for type II endoleaks with GRASP-VIBE compared to TWIST-VIBE scans (AUC: 0.96 *vs.* 0.73; P=0.04). Although diagnostic accuracy improved with GRASP-VIBE for overall endoleak detection (AUC: 0.94 *vs.* 0.79) and endoleak type I detection (AUC: 1.0 *vs.* 0.90), the results were not significant (P≥0.08). Quantitative assessment of different tissues in both MRA sequences demonstrated significantly better SNR for the clotted aneurysm sac, muscle, and bone in the TWIST-VIBE scans. Furthermore, the TWIST-VIBE images had significantly higher muscle-to-bone CNR and muscle-to-fat CNR than in GRASP-VIBE images. However, the SNR measurements in the aorta, fat, and if present in the perfused part of the aneurysm sac did not show significantly different values between the compared sequences. There was no significant difference in CNR regarding measurements of the aortic vessel and the perfused or clotted aneurysm sac.

Contrast-enhanced MR angiography has been shown to be superior to CTA in detecting and classifying endoleaks, especially type II endoleaks (17,19-21). Time-resolved MRA using the conventional dynamic TWIST sequence constitutes an important imaging technique for assessing endoleaks and has been implemented in many published studies (20,22-24). This technique has a high temporal resolution, even higher than the GRASP sequence (TWIST: 2.49 seconds, *vs.* GRASP: 3.1 seconds, *Table 1*).

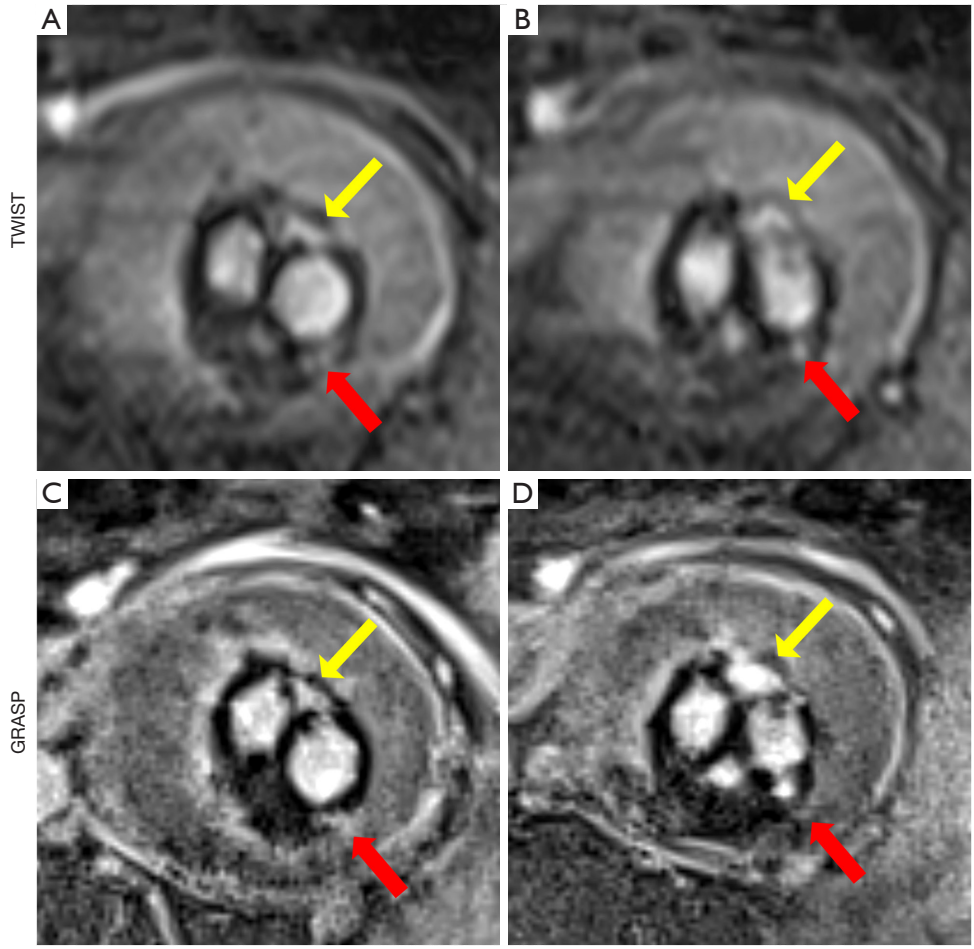

Figure 3 Follow-up imaging after EVAR and iliac in-stent prostheses in a 79-year-old man with an infrarenal abdominal aortic aneurysm. (A,B) Two consecutive axial images acquired by the TWIST sequence showing contrast material in the aneurysm sac (yellow arrows). The red arrows in (A,B) show the contrast material, however, without evident communication to a certain vessel or to the prostheses, which hinders the classification of this endoleak. (C,D) Two consecutive axial images acquired by the GRASP sequence showing contrast material in the aneurysm sac (yellow arrows). The red arrows in (C,D) show the contrast material with communication to the wall of the prostheses, which favors a type II endoleak. It was postulated that the feeding vessel is the left renal artery. Furthermore, note the improved sharpness, decreased motion artifacts and enhanced image quality provided by the GRASP sequence. TWIST, time-resolved angiography with interleaved stochastic trajectories; GRASP, golden-angle radial sparse parallel; EVAR, endovascular aortic aneurysm repair.

Furthermore, the TWIST had a shorter acquisition time than GRASP (2:36 *vs.* 2:54 minutes, *Table 1*). Despite its high temporal resolution, it has been criticized for its high susceptibility to motion artifacts and its low spatial resolution, which limits its performance in detecting small endoleaks (20).

Our findings of the subjective qualitative analysis are concordant with these results showing that the contrast-enhanced GRASP sequence outperformed the contrast-enhanced TWIST sequence. The likely explanation for these results as well as the reason for superior detection of type II endoleaks is the underlying physics principles of these techniques. The GRASP allows for flexible data sorting and retrospective adjustment of temporal resolution, which helps eliminate motion artifacts and reduces the need for patient respiratory cooperation.

In MRA, spatial and temporal resolution are competing factors (25). Visualizing small vessels and minute endoleaks require high spatial resolution. However, delineating dynamic vascular physiologic properties and pathological

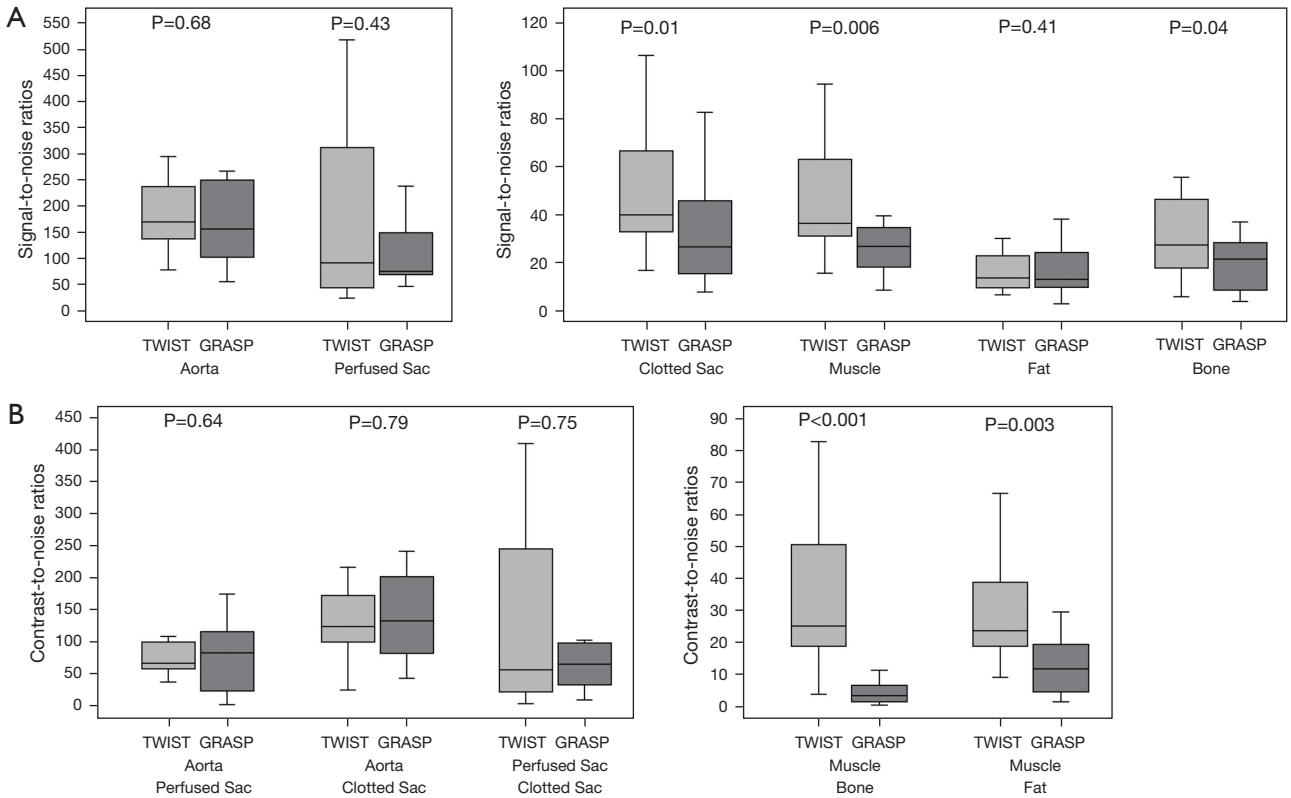

Figure 4 Box and whisker plots of signal-to-noise ratios (A) and contrast-to-noise ratios (B) of different tissues on TWIST-VIBE and GRASP-VIBE sequences. P values are used to assess the relationship between a tissue type on its corresponding sequences. TWIST, time-resolved angiography with interleaved stochastic trajectories; GRASP, golden-angle radial sparse parallel; TWIST-VIBE, time-resolved angiography with interleaved stochastic trajectories-volume interpolated breath-hold examination; GRASP-VIBE, golden-angle radial sparse parallel-volume interpolated breath-hold examination.

entities requires high temporal resolution. To enhance spatial resolution, it's mandatory to sample more k-space data points. Yet, the extended sampling process increases imaging time, consequently compromising temporal resolution (25). To solve this dilemma, many approaches have been developed.

The TWIST is a gradient-echo 3D view-sharing time-resolved MRA technique. The k-space is fully and much more frequently sampled in the center, where image contrast information is prevalent, and under sampled at the periphery (25). However, if these central lines are compromised by motion artifacts, this leads to a notable degradation in image quality.

On the other hand, the GRASP sequence combines parallel imaging, compressed sensing and golden-angle radial sampling, enabling consistent volumetric measurements with sparse filling of k space data (9,12,17,26). This technique involves oversampling and redundant updating of the center of k-space in all directions, which is crucial for correcting potential motion artifacts that could affect the integrity of k-space data. In this method, all spokes contribute to image contrast, rendering it more resistant to motion artifacts (12,26,27). Also, noise resulting from moving anatomical structures is not exhibited as ghosting along a single phase-encoded direction, but rather distributed more uniformly across the entire image (9,12,26,27).

The contrast-enhanced GRASP technique has been established in clinical routine in multiple imaging arenas such as neuroimaging for delineating dynamic contrast flow in pituitary adenomas, cancer staging of head and neck tumors and dynamic MRI of the prostate for upstaging or downstaging of inconclusive prostate lesions (28-30). Most importantly, since it is considered less susceptible to motion artifacts it was initially implemented for dynamic liver imaging, enabling breath-free examinations in patients with

limited breath-hold capacity (31). Despite the advantages of this technique, its clinical translation has not been established in imaging of the postoperative aorta, where temporal components, such as high blood flow in the aorta and slow flow of endoleaks in the aneurysm sac could be dynamically investigated (17).

To our best knowledge, there is only one previous prospective study, which investigated the performance of the contrast-enhanced GRASP sequence in detecting and classifying inconclusive endoleaks as seen on CT angiography. This study showed that the GRASP sequence was clinically feasible, enabling excellent image quality and improved diagnostic confidence in comparison to multiphase CTA, especially in the context of detecting type II endoleaks and in delineating the in- and out-flow arteries communicating with the aneurysm sac (17). Our findings build on the results of the previous study, demonstrating that contrast-enhanced GRASP imaging outperformed conventional TWIST MRA.

This study has limitations. The single-center, single-vendor design, coupled with the exclusive use of 3T scanners for all examinations and a small sample size, restricts the generalizability of our findings. Nonetheless, this study only included patients, who had inconclusive findings on CTA inherently reducing the participant size significantly. Patients with clear evidence of endoleak did not undergo additional imaging, which would otherwise unnecessarily postpone their treatment. Additionally, angiographic intervention, either through selective imaging or intraprocedural cone-beam CT, is traditionally regarded as the ideal reference standard for confirming the presence of an endoleak. Thus, the reference standard was pragmatically selected as a comprehensive integration of radiological and clinical evaluations, coupled with an extensive follow-up period. However, it is important to note that digital subtraction angiography may also miss endoleaks, when non-selective angiography is performed (17,20,22). Furthermore, the slight difference in the temporal resolution of the sequences may influence the results of the image quality and quantitative analyses. Despite the aforementioned limitations, this prospective study provides encouraging preliminary results showing that the contrast-enhanced GRASP sequence may be a valid imaging technique for endoleak detection.

Conclusions

In conclusion, compressed-sensing dynamic GRASP-VIBE sequence, with its superior image quality, diagnostic confidence and performance, may be preferred over the standard TWIST-VIBE sequence in inconclusive endoleak cases. These preliminary findings warrant validation through additional prospective clinical studies involving a larger sample size to confirm external validity.

Acknowledgments

Funding: None.

Footnote

Reporting Checklist: The authors have completed the STARD reporting checklist. Available at https://qims.amegroups.com/article/view/10.21037/qims-24-1130/rc

Conflicts of Interest: All authors have completed the ICMJE uniform disclosure form (available at https://qims.amegroups.com/article/view/10.21037/qims-24-1130/coif). The authors have no conflicts of interest to declare.

Ethical Statement: The authors are accountable for all aspects of the work in ensuring that questions related to the accuracy or integrity of any part of the work are appropriately investigated and resolved. The study received approval from the local institutional review board of the University of Tuebingen (No. 166/2018BO2). All participants provided written informed consent prior to their involvement of the study. The study was conducted in accordance with the Declaration of Helsinki (as revised in 2013).

References

1. Stavropoulos SW, Charagundla SR. Imaging techniques for detection and management of endoleaks after endovascular aortic aneurysm repair. Radiology 2007;243:641-55.

2. van Zandwijk JK, Schuurmann RCL, Haken BT, Stassen CM, Geelkerken RH, de Vries JPM, Simonis FFJ. Endograft position and endoleak detection after endovascular abdominal aortic repair with low-field tiltable MRI: a feasibility study. Eur Radiol Exp 2023;7:82.
3. Smith T, Quencer KB. Best Practice Guidelines: Imaging Surveillance After Endovascular Aneurysm Repair. AJR Am J Roentgenol 2020;214:1165-74.
4. Zaiem F, Almasri J, Tello M, Prokop LJ, Chaikof EL, Murad MH. A systematic review of surveillance after endovascular aortic repair. J Vasc Surg 2018;67:320-331.e37.
5. Williams AB, Williams ZB. Imaging modalities for endoleak surveillance. J Med Radiat Sci 2021;68:446-52.
6. Chen J, Stavropoulos SW. Management of Endoleaks. Semin Intervent Radiol 2015;32:259-64.
7. Kim SM, Ra HD, Min SI, Jae HJ, Ha J, Min SK. Clinical significance of type I endoleak on completion angiography. Ann Surg Treat Res 2014;86:95-9.
8. Pandey N, Litt HI. Surveillance Imaging Following Endovascular Aneurysm Repair. Semin Intervent Radiol 2015;32:239-48.
9. Goldman-Yassen AE, Raz E, Borja MJ, Chen D, Derman A, Dogra S, Block KT, Dehkharghani S. Highly time-resolved 4D MR angiography using golden-angle radial sparse parallel (GRASP) MRI. Sci Rep 2022;12:15099.
10. Korn A, Fenchel M, Hauser TK, Bisdas S, Nägele T, Ernemann U, Klose U, Bender B. Double Bolus Application in TWIST-MR-Angiography of the Cervical Arteries. Radiol Res Pract 2012;2012:203538.
11. Huf VI, Fellner C, Wohlgemuth WA, Stroszczynski C, Schmidt M, Forman C, Wetzl J, Uller W. Fast TWIST with iterative reconstruction improves diagnostic accuracy of AVM of the hand. Sci Rep 2020;10:16355.
12. Feng L, Grimm R, Block KT, Chandarana H, Kim S, Xu J, Axel L, Sodickson DK, Otazo R. Golden-angle radial sparse parallel MRI: combination of compressed sensing, parallel imaging, and golden-angle radial sampling for fast and flexible dynamic volumetric MRI. Magn Reson Med 2014;72:707-17.
13. Feng L, Wen Q, Huang C, Tong A, Liu F, Chandarana H. GRASP-Pro: imProving GRASP DCE-MRI through self-calibrating subspace-modeling and contrast phase automation. Magn Reson Med 2020;83:94-108.
14. Hur SJ, Choi Y, Yoon J, Jang J, Shin NY, Ahn KJ, Kim BS. Intraindividual Comparison between the Contrast-Enhanced Golden-Angle Radial Sparse Parallel Sequence and the Conventional Fat-Suppressed Contrast-Enhanced T1-Weighted Spin-Echo Sequence for Head and Neck MRI. AJNR Am J Neuroradiol 2021;42:2009-15.
15. Feng L. Golden-Angle Radial MRI: Basics, Advances, and Applications. J Magn Reson Imaging 2022;56:45-62.
16. Lustig M, Donoho D, Pauly JM. Sparse MRI: The application of compressed sensing for rapid MR imaging. Magn Reson Med 2007;58:1182-95.
17. Almansour H, Mustafi M, Lescan M, Grosse U, Andic M, Schmehl J, Artzner C, Grözinger G, Walter SS. Dynamic Radial MR Imaging for Endoleak Surveillance after Endovascular Repair of Abdominal Aortic Aneurysms with Inconclusive CT Angiography: A Prospective Study. J Clin Med 2024;13:2913.
18. Chun JY, de Haan M, Maleux G, Osman A, Cannavale A, Morgan R. CIRSE Standards of Practice on Management of Endoleaks Following Endovascular Aneurysm Repair. Cardiovasc Intervent Radiol 2024;47:161-76.
19. Engellau L, Larsson EM, Albrechtsson U, Jonung T, Ribbe E, Thörne J, Zdanowski Z, Norgren L. Magnetic resonance imaging and MR angiography of endoluminally treated abdominal aortic aneurysms. Eur J Vasc Endovasc Surg 1998;15:212-9.
20. Habets J, Zandvoort HJ, Reitsma JB, Bartels LW, Moll FL, Leiner T, van Herwaarden JA. Magnetic resonance imaging is more sensitive than computed tomography angiography for the detection of endoleaks after endovascular abdominal aortic aneurysm repair: a systematic review. Eur J Vasc Endovasc Surg 2013;45:340-50.
21. Haulon S, Lions C, McFadden EP, Koussa M, Gaxotte V, Halna P, Beregi JP. Prospective evaluation of magnetic resonance imaging after endovascular treatment of infrarenal aortic aneurysms. Eur J Vasc Endovasc Surg 2001;22:62-9.
22. Cohen EI, Weinreb DB, Siegelbaum RH, Honig S, Marin M, Weintraub JL, Lookstein RA. Time-resolved MR angiography for the classification of endoleaks after endovascular aneurysm repair. J Magn Reson Imaging 2008;27:500-3.
23. Lookstein RA, Goldman J, Pukin L, Marin ML. Time-resolved magnetic resonance angiography as a noninvasive method to characterize endoleaks: initial results compared with conventional angiography. J Vasc Surg 2004;39:27-33.
24. van der Laan MJ, Bakker CJ, Blankensteijn JD, Bartels LW. Dynamic CE-MRA for endoleak classification after endovascular aneurysm repair. Eur J Vasc Endovasc Surg 2006;31:130-5.
25. Blackham KA, Passalacqua MA, Sandhu GS, Gilkeson RC, Griswold MA, Gulani V. Applications of time-resolved MR angiography. AJR Am J Roentgenol 2011;196:W613-20.

26. Chandarana H, Block TK, Rosenkrantz AB, Lim RP, Kim D, Mossa DJ, Babb JS, Kiefer B, Lee VS. Free-breathing radial 3D fat-suppressed T1-weighted gradient echo sequence: a viable alternative for contrast-enhanced liver imaging in patients unable to suspend respiration. Invest Radiol 2011;46:648-53.
27. Block KT, Chandarana H, Milla S, Bruno M, Mulholland T, Fatterpekar G, Hagiwara M, Grimm R, Geppert C, Kiefer B, Sodickson DK. Towards Routine Clinical Use of Radial Stack-of-Stars 3D Gradient-Echo Sequences for Reducing Motion Sensitivity. J Korean Soc Magn Reson Med 2014;18:87-106.
28. Hainc N, Stippich C, Reinhardt J, Stieltjes B, Blatow M, Mariani L, Bink A. Golden-angle radial sparse parallel (GRASP) MRI in clinical routine detection of pituitary microadenomas: First experience and feasibility. Magn Reson Imaging 2019;60:38-43.
29. Mogen JL, Block KT, Bansal NK, Patrie JT, Mukherjee S, Zan E, Hagiwara M, Fatterpekar GM, Patel SH. Dynamic Contrast-Enhanced MRI to Differentiate Parotid Neoplasms Using Golden-Angle Radial Sparse Parallel Imaging. AJNR Am J Neuroradiol 2019;40:1029-36.
30. Winkel DJ, Heye TJ, Benz MR, Glessgen CG, Wetterauer C, Bubendorf L, Block TK, Boll DT. Compressed Sensing Radial Sampling MRI of Prostate Perfusion: Utility for Detection of Prostate Cancer. Radiology 2019;290:702-8.
31. Weiss J, Ruff C, Grosse U, Grözinger G, Horger M, Nikolaou K, Gatidis S. Assessment of Hepatic Perfusion Using GRASP MRI: Bringing Liver MRI on a New Level. Invest Radiol 2019;54:737-43.

Cite this article as: Almansour H, Mustafi M, Lescan M, Grosse U, Andic M, Schmehl J, Artzner C, Grözinger G, Walter SS. Golden-angle radial sparse parallel (GRASP) magnetic resonance angiography (MRA) for endoleak evaluation after endovascular repair of the aorta: a prospective comparison to conventional time-resolved MRA. Quant Imaging Med Surg 2024;14(10):7420-7432. doi: 10.21037/qims-24-1130